ARM Aerial Facility (AAF) Merged Value-Added Product Report for Historical G-1 Field Campaigns

F Mei   K Gaustad

March 2024

DISCLAIMER

ARM Aerial Facility (AAF) Merged Value-Added Product Report for Historical G-1 Field Campaigns

F Mei
K Gaustad
Both at Pacific Northwest National Laboratory

March 2024

Acronyms and Abbreviations

AAF	ARM Aerial Facility
AAFMERGED VAP	ARM Aerial Facility Merged Value-Added Product
ACE-ENA	Aerosol and Cloud Experiments in the Eastern North Atlantic
ACME-V	Airborne Carbon Measurements-V
ADC	ARM Data Center
ADI	ARM Data Integrator
AMS	time-of-flight aerosol mass spectrometer
ARM	Atmospheric Radiation Measurement
BBOP	Biomass Burning Observation Project
CACTI	Cloud, Aerosol, and Complex Terrain Interactions
CAS	cloud and aerosol spectrometer
CCN	cloud condensation nuclei
CF	climate forecast
CVI	counterflow virtual impactor
DOD	data object definition
DOE	U.S. Department of Energy
FCDP	fast cloud droplet probe
FIMS	fast integrated mobility spectrometer
G-1	Gulfstream-1 aircraft
GMT	Greenwich Mean Time
GoAmazon	Green Ocean Amazon
HI-SCALE	Holistic Interactions of Shallow Clouds, Aerosols, and Land-Ecosystems
IWGADTS	Inter-agency Working Group for Airborne Data and Telemetry Systems
netCDF	network Common Data Form
NGA	National Geospatial-Intelligence Agency
PCASP	passive-cavity aerosol spectrometer
PCM	processing configuration manager
RH	relative humidity
SGP	Southern Great Plains
STP	standard temperature and pressure
TAS	true airspeed
VAP	value-added product

Contents

Figures

Tables

1.0   Introduction

For 30 years, the U.S. Department of Energy (DOE) Office of Science supported an instrumented Grumman Gulfstream-1 (G-1) aircraft for atmospheric field campaigns. Data from the final decade of G-1 operations were archived by the Atmospheric Radiation Measurement (ARM) user facility Data Center (ADC) and made publicly available at no cost to all registered users. To ensure a consistent data format and to improve the accessibility of the ARM airborne data, an integrated data set was recently developed covering the final six years of G-1 operations (2013 to 2018). The integrated data set includes data collected from 236 flights (766.4 hours).

Four of the seven field campaigns were based in the U.S. One campaign collected data from the wildfires in the U.S. Pacific Northwest and agricultural burns in the lower Mississippi River valley as part of the Biomass Burning Observation Project (BBOP) in 2013. In 2015, the ARM Cloud Aerosol Precipitation Experiment provided data on atmospheric rivers and associated aerosol-cloud interactions that produce heavy precipitation on the U.S. west coast during the early spring. Research data from Airborne Carbon Measurements-V (ACME-V), collected during the summer of 2015, gave scientists insight into trends and variability of trace gases in the atmosphere over the North Slope of Alaska to improve arctic climate models. In the early summer and autumn of 2016, the Holistic Interactions of Shallow Clouds, Aerosols, and Land-Ecosystems (HI-SCALE) campaign provided an extensive data set geared toward coupled processes that affect the life cycle of shallow clouds through the interaction among aerosol, cloud, land surface, and ecosystems.

In 2014 (March and October), the airborne sampling moved outside of the U.S. to the city of Manaus in central Amazonia, Brazil, where residential and industrial emissions were extensively characterized by flights of the G-1. The GoAmazon2014/15 aircraft campaign data are being integrated with aquatic and terrestrial ecosystem measurements to quantify anthropogenic perturbations to a usually pristine tropical environment. Another international airborne mission was carried out in the Eastern North Atlantic region. The Aerosol and Cloud Experiments in the Eastern North Atlantic (ACE-ENA) campaign saw the G-1 aircraft fly from Terceira Island in the Azores during the summer of 2017 and the winter of 2018. The campaign studied both seasons to measure key aerosol and cloud processes under various meteorological and cloud conditions with different aerosol sources. Then the G-1 deployed to the Sierras de Córdoba range in central Argentina from October to November 2018 for the Cloud, Aerosol, and Complex Terrain Interactions (CACTI) campaign to study orographic convective cloud interactions with their surrounding environment.

These comprehensive datastreams provide much-needed insight into spatiotemporal variability of thermodynamic quantities, aerosol and cloud states, and properties for addressing essential science questions in Earth system process studies.

2.0   Algorithm and Methodology

The ARM data system uses a multi-tiered data processing approach (Prakash et al. 2016) that iteratively processes the instrument data to produce higher-level data products. Data is first processed from the instrument's raw data format (data level 00) to netCDF format. During this initial processing, conversion of geophysical units and application of calibration factors is performed as appropriate (documented in a-

and b level data products). Quality controls can also be applied (creating b1-level data files). Additional processing can be added to further increase the level of these files with 'higher value' to store as a data level 'c1'. For example, mentor-edited data files with additional quality improvement calibration are usually considered the 'c'-level data product.

The content of ARM data files is structured in three main sections: dimensions, variables, and global attributes. As time-series measurements, the time dimension of ARM products is considered 'unlimited'. Per netCDF3 requirements, the unlimited dimension 'time' is the first dimension of a variable that uses the time dimension. The variables encompass coordinate variables reporting dimension values, primary measurements (recommended for scientific use), supporting measurements (e.g., diagnostics and quality), and location variables detailing latitude, longitude, and altitude. Variables are equipped with supporting attributes to facilitate the user's understanding and interpretation. These include a "long_name" for unique descriptions, "units" conforming to unit conventions, and a "missing_value" to represent no data. A "standard_name" attribute, following the Climate Forecast (CF) standard, is assigned when applicable. The final section in ARM netCDF files consists of global attributes containing information related to the platform's location, time interval, calibration procedures (if available), and contact information for instrument mentors or principal investigators.

A final merged product (aafmerged.c1) was created to provide users with all G-1 airborne measurements in a single netCDF file that follows ARM data standards. This merged data product is produced using the ARM Data Integrator (ADI, https://github.com/ARM-DOE/ADI), a framework designed to automate data retrieval, integration, and the creation of time-series netCDF data products. ADI allows users to seamlessly combine data products, extract specific variables, and transform them into user-defined coordinate systems. The time dimension of the merged data product aligns with the input aafnaviwg.c1 datastream. All other instrument data were mapped onto the aafnaviwg.c1 sampling period using ADI's nearest-neighbor transformation method.

3.0   Input Data

Input data to the ARM Aerial Facility Merged Value-Added Product (AAFMERGED VAP) include aerosol, cloud, and trace gas measurements; meteorological properties; and geophysical location data. These are retrieved from up to 23 ARM data products depending on availability of these datastreams at a given site and period. A list of all possible input datastreams, their data level(s), a general description of the data source, and the datastream's measurements integrated into the AAFMERGED VAP are provided in Table 1.

Table 1.   Input datastream name, level, description, and measurements retrieved.

Input Datastream Name (instrument + qualifier)	Data Levels	Datastream Description	Measurement Descriptions
aaf2dsh	c1	2-dimensional stereo probe – horizontal	Cloud particle size distribution 10 to 3,000 μm
aaf2dsv	c1	2-dimensional stereo probe – vertical	Cloud particle size distribution 10 to 3,000 μm
aafams	b1	Time-of-flight aerosol mass spectrometer (AMS)	Particle chemical composition/trace gas measurements

Input Datastream Name (instrument + qualifier)	Data Levels	Datastream Description	Measurement Descriptions
aafccn2cola	b1	Cloud condensation nuclei counter (dual column), ramping mode	Concentration of cloud condensation nuclei at two specified supersaturations
aafccn2colb	b1	Cloud condensation nuclei counter (dual column), non-ramping mode	Concentration of cloud condensation nuclei at two specified supersaturations
aafcpcfcvi	a1, b1	Condensation particle counter via CVI inlet	Total aerosol concentration >0.010 µm
aafcpcfiso	a1, b1	Condensation particle counter via isokinetic inlet	Total aerosol concentration >0.010 µm
aafcpcu	a1, b1	Ultrafine condensation particle counter	Total aerosol concentration >0.003 µm
aafcdp	c1	Cloud droplet probe	Aerosol concentration
aaffims	b1	Fast integrating mobility spectrometer	Aerosol size distribution 0.010 to 0.450 µm
aafhvps	c1	High-volume precipitation spectrometer	Cloud particle size distribution 150 to 19,600 µm
aafinletcvi	c1	Counterflow virtual impactor inlet	Sampling of cloud droplet residuals
aafinletisok	a1	Isokinetic inlet	Sample stream of dry aerosol, sizes < 5 µm
aafmergedaerosolsd	c1	Merged aerosol size distribution	Aerosol particle size distribution
aafmergedcldsd	c1	Merged cloud size distribution	Cloud particle size distribution/Cloud particle number concentration
aafnaviwg	c1	Navigation and met data from IWGADTS	Meteorological properties and geophysical location measurements
aafneph	a1, b1	Nephelometer	Aerosol scattering coefficient 450, 550, 700 nm wavelengths
aafo3	a1, c1	Ozone monitor	Ozone concentration
aafpcasp	a1	Passive-cavity aerosol spectrometer	Size distribution 0.10 to 3 µm
aafpsap1s	b1	Particle soot absorption photometer absorption coefficients	Aerosol absorption coefficient 462, 523, 648 nm wavelengths
aafso2	a1, c1	Sulfur dioxide monitor	Sulfer dioxide concentration
aafsp2rbc10s	c1	Single-particle soot photometer refractory black carbon: 10-second, aboard aircraft	Soot spectrometry
aafuhsas	a1	Ultra-high-sensitivity aerosol spectrometer	Aerosol size distribution 0.060 to 1 µm

3.1   Flow Chart

ARM processing configuration manager (PCM) provides tools to gather and store the VAP process and output data object definition (DOD) of ARM VAPs. The process definition includes documenting all possible input data sources, how to map retrieved input data to specific output variables, and the transformation technique to apply to consolidate the input data onto a common output coordinate grid. This information gathered via the PCM is stored in the data system database (dsdb), which is accessed by the ARM Data Integrator (ADI) when VAPs are executed. The nearest-neighbor transformation method used by the AAFMERGED VAP supports the use of a range transformation parameter that allows specifying a time range within which the next 'good' sample will be used when the closest sample in the input data to the target output time is bad or missing. A range of up to 30 minutes is used for all input datastreams except the aafams.b1. For the aafmas.b1 (i.e., time-of-flight aerosol mass spectrometer [AMS]) the maximum range permitted to associate an input sample to output target time is 14s.

A high-level flow diagram illustrating the measurements and PCM definitions feeding the ARM Data Integrator libraries to produce the AAFMERGED output product is shown in Figure 1. The AAFMERGED VAP does not apply any special algorithms or perform scientific analysis on the data retrieved and transformed. The VAPs sole purpose is to create a consolidated data product that simplifies a user's ability to access and use the AAF data products.
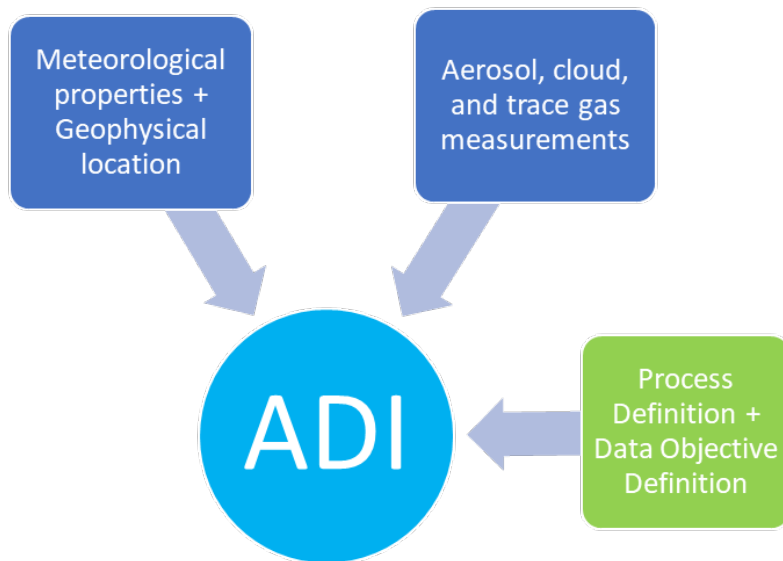
Figure 1.   High-level data and process flow diagram.

Figure 2 shows a more detailed flow diagram that documents how the VAP iterates over each input aafnaviwg.c1data file, transforms all other data onto the naviwg.c1 time grid using a nearest-neighbor approach, creating an output file and quicklook plots of key, one dimensional, measurements. Sample quicklooks of the AAFMERGED VAP variables ambient_temperature and cpcu_concentration from the CACTI campaign are provided in Figure 3 and Figure 4 respectively.

Figure 2.   Detailed process flow diagram of AAFMERGED VAP.

Figure 3.   Ambient temperature from CACTI on flight initiated on December 7, 2018 at 15:01:17 GMT.
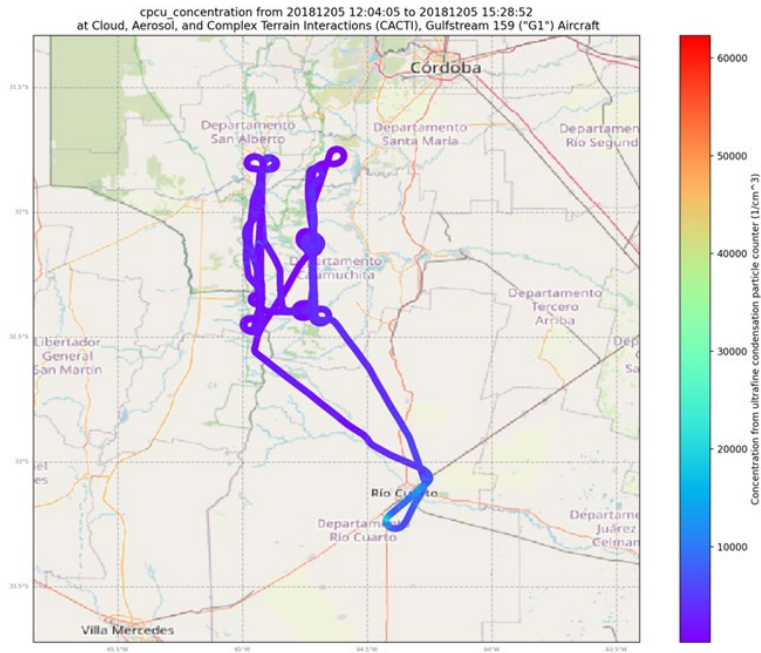
Figure 4.   Concentration from ultrafine condensation particle counter from CACTI flight initiated on December 5, 2018 at 15:28:52 GMT.

4.0   Output Data

The AAFMERGED VAP produces one output file, named:

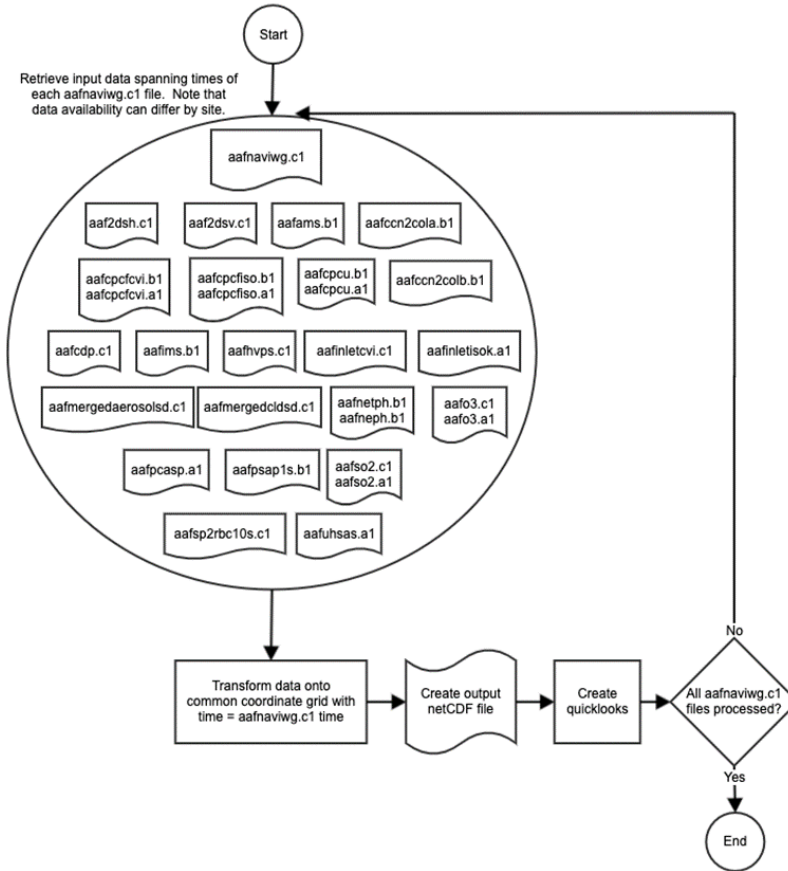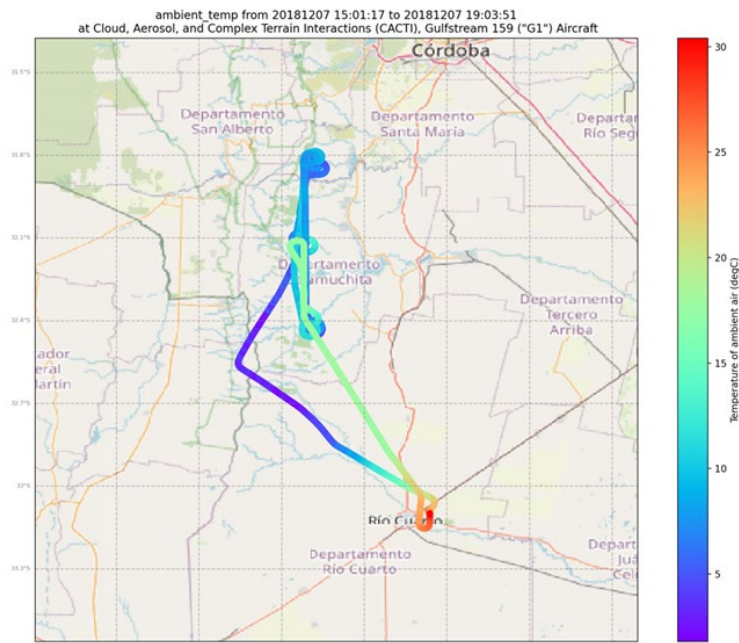SSSaafmergedXX.c1.YYYYMMDD.hhmmss.nc

Where:

• SSS is the site of the instrument (e.g., SGP)
• XX is the facility (i.e., C1, C2, etc.)
• YYYY is the year
• MM is the month of the year
• DD is the day of the month
• hh is the hour of the day
mm is the minute of the hour
ss is the second of the minute.

The time stamps of the output files match those of the aafnaviwg.c1 input files because the output target time is the same as the aafnaviwg.c1 sample times. Thus, if there is no aafnaviwg.c1 data for a given period, there will be no aafmerged data for that same period. An aafmerged file is produced for each G-1 aircraft flight for a given atmospheric field campaign. More than one flight may occur over the course of a single day, producing an aafmerged output file for each of these flights. Non-time dimensions of all inputs are propagated to the output file unchanged. Not all datastreams are available at all campaigns. All possible variables, their dimensions, and associated long-name descriptions that can make up an

aafmerged.c1output are listed in Table 2. Primary measurements are noted in bold. Quicklooks are produced for all primary variables.

Table 2. Output variable names and descriptions.

Output Variable Name	Output Variable Description
base_time	Base time in Epoch
time_offset	Time offset from base_time
time	Time offset from midnight
aaf2dsh_optical_diameter	Optical diameter from two-dimensional stereo probe sh
aaf2dsh_optical_diameter_bounds	Optical diameter bounds from two-dimensional stereo probe sh
aaf2dsv_optical_diameter	Optical diameter from two-dimensional stereo probe sv
aaf2dsv_optical_diameter_bounds	Optical diameter bounds from two-dimensional stereo probe sv
cdp_optical_diameter	Optical diameter from fast cloud droplet probe
cdp_optical_diameter_bounds	Optical diameter bounds from fast cloud droplet probe
fims_geometric_diameter	Geometric diameter from fast integrating mobility spectrometer
fims_geometric_diameter_bounds	Geometric diameter bounds from fast integrating mobility spectrometer
hvps_optical_diameter	Optical diameter from high-volume precipitation spectrometer
hvps_optical_diameter_bounds	Optical diameter bounds from high-volume precipitation spectrometer
aerosolsd_geometric_diameter	Geometric diameter from merged aerosol size distribution
aerosolsd_geometric_diameter_bounds	Geometric diameter bounds from merged aerosol size distribution
cldsd_optical_diameter	Optical diameter
cldsd_optical_diameter_bounds	Optical diameter bounds
pcasp_optical_diameter	Optical diameter from passive-cavity aerosol spectrometer
pcasp_optical_diameter_bounds	Optical diameter bounds from passive-cavity aerosol spectrometer
sp2_diameter_geo	Mean volume-equivalent geometric diameter
sp2_diameter_geo_bounds	Mean volume-equivalent geometric diameter cell bounds
twodsh_number_concentration	Number concentration from two-dimensional stereo probe sh
twodsh_total_number_concentration	Total number concentration from two-dimensional stereo probe sh
twodsv_number_concentration	Number concentration from two-dimensional stereo probe sv
twodsv_total_number_concentration	Total number concentration from two-dimensional stereo probe sv
ams_alt	Altitude above mean sea level from time-of-flight aerosol mass spectrometer
ams_Chl	Chloride mass concentration from time-of-flight aerosol mass spectrometer
ams_Chl_err	Chloride mass concentration error from time-of-flight aerosol mass spectrometer
ams_CVI_enhancement_factor	CVI enhancement factor from time-of-flight aerosol mass spectrometer
ams_flag	Flag from time-of-flight aerosol mass spectrometer
ams_lat	North latitude from time-of-flight aerosol mass spectrometer
ams_lon	East longitude from time-of-flight aerosol mass spectrometer
ams_NH4	Ammonium mass concentration from time-of-flight aerosol mass spectrometer
ams_NH4_err	Ammonium mass concentration error from time-of-flight aerosol mass spectrometer
ams_NO3	Nitrate mass concentration from time-of-flight aerosol mass spectrometer
ams_NO3_err	Nitrate mass concentration error from time-of-flight aerosol mass spectrometer
ams_Org	Organic mass concentration from time-of-flight aerosol mass spectrometer

Output Variable Name	Output Variable Description
ams_Org_err	Organic mass concentration error from time-of-flight aerosol mass spectrometer
ams_SO4	Sulfate mass concentration from time-of-flight aerosol mass spectrometer
ams_SO4_err	Sulfate mass concentration error from time-of-flight aerosol mass spectrometer
ccna_N_CCN	Number concentration of CCN from cloud condensation nuclei counter a
ccna_P_sample	Sample pressure of CCN from cloud condensation nuclei counter a
ccna_supersaturation_calculated	Sample supersaturation calculated via Lance/Rose method from cloud condensation nuclei counter a
ccna_temp_unstable	Logical value, indicating whether the instrument has reached thermal gradient stabilization and is within 0.4 degrees C of the set point from cloud condensation nuclei counter a
ccna_T_inlet	Temperature read of sample air at entrance to instrument from cloud condensation nuclei counter a
ccna_T_sample	Temperature read of sample air entering the column from cloud condensation nuclei counter a
ccnb_N_CCN	Number concentration of CCN from cloud condensation nuclei counter b
ccnb_P_sample	Sample pressure from cloud condensation nuclei counter b
ccnb_supersaturation_calculated	Sample supersaturation calculated via Lance/Rose method from cloud condensation nuclei counter b
ccnb_temp_unstable	Logical value, indicating whether the instrument has reached thermal gradient stabilization and is within 0.4 degrees C of the set point from cloud condensation nuclei counter b
ccnb_T_inlet	Temperature read of sample air at entrance to instrument from cloud condensation nuclei counter b
ccnb_T_sample	Temperature read of sample air entering the column from cloud condensation nuclei counter b
cpcfcvi_concentration	Particle concentration from condensation particle counter via cvi inlet
cpcfiso_concentration	Particle concentration from condensation particle counter via isokinetic inlet
cpcu_concentration	Concentration from ultrafine condensation particle counter
fcdp_number_concentration	Number concentration from fast cloud droplet probe
fcdp_total_number_concentration	Total number concentration from fast cloud droplet probe
fims_alt	Altitude above mean sea level from fast integrating mobility spectrometer
fims_heated_flag	Flag indicating if the data is heated or unheated from fast integrating mobility spectrometer
fims_lat	North latitude from fast integrating mobility spectrometer
fims_lon	East longitude from fast integrating mobility spectrometer
fims_number_concentration	Number concentration from fast integrating mobility spectrometer
fims_pressure	Ambient pressure from fast integrating mobility spectrometer
fims_temperature	Ambient temperature from fast integrating mobility spectrometer
hvps_number_concentration	Number concentration from high-volume precipitation spectrometer
hvps_total_number_concentration	Total number concentration from high-volume precipitation spectrometer
inletcvi_cvi_cut_size	CVI cut size from counterflow virtual impactor inlet
inletcvi_enhancement_factor	CVI enhancement factor from counterflow virtual impactor inlet
inletcvi_inlet_dilution_factor	Inlet dilution factor for under-kinetic mode from counterflow virtual impactor inlet
inletcvi_inlet_selector	Inlet selector valve position from counterflow virtual impactor inlet
inletisok_cabin_temperature	Cabin temperature from facility isokinetic inlet

Output Variable Name	Output Variable Description
inletisok_pressure_isok_inlet	Pressure at isokinetic inlet manifold from facility isokinetic inlet
inletisok_relative_humidity_isok_inlet	Relative humidity at isokinetic inlet manifold from facility isokinetic inlet
inletisok_temperature_isok_inlet	Temperature at isokinetic inlet manifold from facility isokinetic inlet
aerosolsd_alt	Altitude above mean sea level from merged aerosol size distribution
aerosolsd_cas_flag	CAS flag from merged aerosol size distribution
aerosolsd_cloud_flag	Cloud flag from merged aerosol size distribution
aerosolsd_cvi_flag	CVI flag from merged aerosol size distribution
aerosolsd_fcdp_flag	FCDP flag from merged aerosol size distribution
aerosolsd_fims_flag	FIMS flag from merged aerosol size distribution
aerosolsd_lat	North latitude from merged aerosol size distribution
aerosolsd_lon	East longitude from merged aerosol size distribution
aerosolsd_number_concentration	Number concentration from merged aerosol size distribution
aerosolsd_pcasp_flag	PCASP flag from merged aerosol size distribution
cldsd_alt	Altitude above mean sea level from merged cloud size distribution
cldsd_lat	North latitude from merged cloud size distribution
cldsd_lon	East longitude from merged cloud size distribution
cldsd_number_concentration	Number concentration from merged cloud size distribution
cldsd_total_number_concentration	Total number concentration from merged cloud size distribution
neph_Bbs_B	Aerosol back-hemispheric light-scattering coefficient, nominal blue wavelength from nephelometer
neph_Bbs_G	Aerosol back-hemispheric light-scattering coefficient, nominal green wavelength from nephelometer
neph_Bbs_R	Aerosol back-hemispheric light-scattering coefficient, nominal red wavelength from nephelometer
neph_Bs_B	Aerosol total light-scattering coefficient, nominal blue wavelength from nephelometer
neph_Bs_G	Aerosol total light-scattering coefficient, nominal green wavelength from nephelometer
neph_Bs_R	Aerosol total light-scattering coefficient, nominal red wavelength from nephelometer
neph_P_sample	Pressure inside nephelometer
neph_RH_sample	Relative humidity inside nephelometer
neph_T_inlet	Temperature at nephelometer inlet
neph_T_sample	Sample temperature inside nephelometer
pcasp_sample_flow_rate	Sample flow rate from passive-cavity aerosol spectrometer
pcasp_sheath_flow_rate	Sheath flow read from passive-cavity aerosol spectrometer
pcasp_size_distribution	Particle size distribution from passive-cavity aerosol spectrometer
psap_Ba_B_Weiss	Aerosol light absorption coefficient, blue channel at dry or reference RH from particle soot absorption photometer
psap_Ba_G_Weiss	Aerosol light absorption coefficient, green channel at dry or reference RH from particle soot absorption photometer
psap_Ba_R_Weiss	Aerosol light-absorption coefficient, red channel at dry or reference RH from particle soot absorption photometer
sp2_N_dN_rBC	Number density of particles containing refractory black carbon from soot photometer refractory black carbon
sp2_rBC	Refractory black carbon concentration from soot photometer refractory black carbon
o3	Ozone concentration at STP
uhsas_flow	Flow measurement from ultra-high-sensitivity aerosol spectrometer
uhsas_sample_flow_rate	Sample flow rate from ultra-high-sensitivity aerosol spectrometer
uhsas_sample_pressure	Sample pressure from ultra-high-sensitivity aerosol spectrometer
uhsas_sheath_flow	Sheath flow rate from ultra-high-sensitivity aerosol spectrometer
uhsas_lower_size_limit	Lower particle size limit for each bin from ultra-high-sensitivity aerosol spectrometer

Output Variable Name	Output Variable Description
uhsas_upper_size_limit	Upper particle size limit for each bin
uhsas_size_distribution	Particle size distribution, bounded by lower_size_limit and upper_size_limit from ultra-high-sensitivity aerosol spectrometer
so2	Sulfur dioxide (SO2) mixing ratio calculated with nominal sensitivity correction
ambient_temp	Temperature of ambient air
angle_of_attack	Direction of wind relative to aircraft pitch
cabin_pressure	Cabin pressure
cabin_temperature	Cabin temperature
dewpoint_temperature	Dewpoint temperature
dynamic_pressure	Dynamic pressure
ground_speed	Platform speed over the ground
indicated_airspeed	Platform airspeed calculated based on the TAS and static temperature measured by Aimms-20
leg_number	Number of flight leg aircraft is on
pitch	Pitch angle of platform
potential_temperature	Potential temperature calculated from ambient temperature and pressure
press_alt	Altitude calculated from U.S. standard atmospheric tables
radar_alt	Altitude calculated using GPS altitude and position with the Digital Terrain Elevation Data sets from NGA
relative_humidity_ice	Relative humidity relative to ice
relative_humidity_water	Relative humidity relative to water
roll	Roll angle of platform
side_slip	Direction of wind relative to true heading
solar_zenith_ground	Solar zenith
static_pressure	Static pressure
sun_azimuth_aircraft	Sun azimuth at aircraft
sun_azimuth_ground	Sun azimuth at ground level
sun_elev_aircraft	Sun elevation at aircraft
total_temp	Total temperature
true_airspeed	Platform airspeed through the air
true_heading	Platform direction with respect to true north
vertical_velocity	Platform vertical velocity defined in the body frame
vert_wind_speed	Vertical wind speed
wgs_alt	Altitude above the ellipsoid based on WGS-84
wind_direction	Wind direction
wind_speed	Wind speed
lat	North latitude
lon	East longitude
alt	Altitude above mean sea level

5.0 Summary

The combined observational data from these field campaigns facilitates studying of atmospheric processes, such as boundary-layer processes, aerosol-cloud-precipitation interactions, and land-atmosphere-cloud interactions across a wide range of conditions. Although many previous studies have benefited from the G-1 field campaign data (Berg et al. 2020, Creamean et al. 2018, Fast et al. 2019, Gu et al. 2017, Shrivastava et al. 2019, Wang et al. 2022, 2023, Yeom et al. 2021, Zhang et al. 2021, 2023), more manageable data access should support new users in the research community. By incorporating data from multiple sources, these ARM data sets and open-source tools can provide more accurate and reliable information and assist model simulation/prediction improvement. Overall, a merged

airborne aerosol, cloud, and trace gas data set covering seven field campaigns is a powerful tool for atmospheric scientists, supporting a more comprehensive understanding of atmosphere processes impacting the climate. We hope our efforts will encourage broader use of ARM data and enhance collaboration between the ARM user facility and the atmospheric science community.

6.0   References

Berg, LK, CN Long, EI Kassianov, D Chand, S-L Tai, Z Yang, LD Riihimaki, SC Biraud, J Tagestad, A Matthews, A Mendoza, F Mei, J Tomlinson, and JD Fast. 2020. "Fine-Scale Variability of Observed and Simulated Surface Albedo over the Southern Great Plains." *Journal of Geophysical Research – Atmospheres* 125(7): e2019JD030559, https://doi.org/10.1029/2019JD030559

Creamean, JM, M Maahn, G de Boer, A McComiskey, AJ Sedlacek, and Y Feng. 2018. "The influence of local oil exploration and regional wildfires on summer 2015 aerosol over the North Slope of Alaska." *Atmospheric Chemistry and Physics* 18(2): 555–570, https://doi.org/10.5194/acp-555-2018

Fast, JD, LK Berg, L Alexander, D Bell, E D'Ambro, J Hubbe, C Kuang, J Liu, C Long, A Matthews, F Mei, R Newsom, Mikhail Pekour, T Pinterich, B Schmid, S Schobesberger, J Shilling, JN Smith, S Springston, K Suski, JA Thornton, J Tomlinson, J Wang, H Xiao, and A Zelenyuk 2019. "Overview of the HI-SCALE Field Campaign: A New Perspective on Shallow Convective Clouds." *Bulletin of the American Meteorological Society* 100(5): 821–840, https://doi.org/10.1175/BAMS-D-18-0030.2

Gu, D, AB Guenther, JE Shilling, H Yu, M Huang, C Zhao, Q Yang, ST Martin, P Artaxo, S Kim, R Seco T Stavrakou, KM Longo, J Tóta, RAF de Souza, O Vega, Y Liu, M Shrivastava, EG Alves, FC Santos, G Leng, and Z Hu. 2017. "Airborne observations reveal elevational gradient in tropical forest isoprene emissions." *Nature Communications* 8: 15541, https://doi.org/10.1038/ncomms15541

Prakash, G, J Kumar, E Rush, R Records, A Clodfelter, and J Voyles. 2016. "HPC infrastructure to support the next-generation ARM facility data operations." *2016 IEEE International Conference on Big Data (Big Data)*, 4026-4028, https://doi.org/10.1109/BigData.2016.7841098

Shrivastava, M, MO Andreae, P Artaxo, HMJ Barbosa, LK Berg, J Brito, J Ching, RC Easter, J Fan, JD Fast, Z Feng, JD Fuentes, M Glasius, AH Goldstein, EG Alves H Gomes D Gu, A Guenther, SH Jathar, S Kim, Y Liu, S Lou, ST Martin, V Faye McNeill, A Medeiros, SS de S, JE Shilling, SR Springston, RAF Souza, JA Thornton, G Isaacman-VanWertz, LD Yee, R Ynoue, RA Zaveri, A Zelenyuk, and C Zhou. 2019. "Urban pollution greatly enhances formation of natural aerosols over the Amazon rainforest." *Nature Communications* 10: 1046, https://doi.org/10.1038/s41467-019-08909-4

Wang, J, R Wood, MP Jensen, JC Chiu, Y Liu, K Lamer, N Desai, SE Giangrande, DA Knopf, P Kollias, A Laskin, X Liu, C Lu, D Mechem, F Mei, M Starzec, J Tomlinson, Y Wang, SS Yum, G Zheng, AC Aiken, EB Azevedo, Y Blanchard, S China, X Dong, F Gallo, S Gao, VP Ghate, S Glienke, L Goldberger, JC Hardin, C Kuang, EP Luke, AA Matthews, MA Miller, R Moffet, M Pekour, B Schmid, AJ Sedlacek, RA Shaw, JE Shilling, A Sullivan, K Suski, DP Veghte, R Weber, M Wyant, J Yeom, M Zawadowica, and Z Zhang. 2022. "Aerosol and Cloud Experiments in the Eastern North Atlantic (ACE-ENA)." *Bulletin of the American Meteorological Society*103(2): E619-E641, https://doi.org/10.1175/BAMS-D-19-0220.1

Wang, Y, CB Ramesh, SE Giangrande, J Fast, X Gong, J Zhang, AT Odabasi, MVB Oliveira, A Matthews, F Mei, JE Shilling, J Tomlinson, D Wang, and J Wang. 2023. "Examining the vertical heterogeneity of aerosols over the Southern Great Plains." *Atmospheric Chemistry and Physics* 23(24): 15671–15691, https://doi.org/10.5194/acp-23-15671-2023

Yeom, JM, SS Yum, RA Shaw, I La, J Wang, C Lu, Y Liu, F Mei, B Schmid, and A Matthews. 2021. "Vertical Variations of Cloud Microphysical Relationships in Marine Stratocumulus Clouds Observed during the ACE-ENA Campaign." *Journal of Geophysical Research – Atmospheres* 126(24): e2021JD034700, https://doi.org/10.1029/2021JD034700

Zhang, D, AM Vogelmann, F Yang, E Luke, P Kollias, Z Wang, P Wu, WI Gustafson Jr., F Mei, S Glienke, J Tomlinson, and N Desai. 2023. "Evaluation of four ground-based retrievals of cloud droplet number concentration in marine stratocumulus with aircraft in situ measurements." *Atmospheric Measurement Techniques* 16(23): 5827–5846, https://doi.org/10.5194/amt-16-5827-2023

Zhang, Z, Q Song, DB Mechem, VE Larson, J Wang, Y Liu, MK Witte, X Dong, and P Wu. 2021. "Vertical dependence of horizontal variation of cloud microphysics: observations from the ACE-ENA field campaign and implications for warm-rain simulation in climate models." *Atmospheric Chemistry and Physics* 21(4): 3103–3121, https://doi.org/10.5194/acp-21-3103-2021